Title

Feasibility Study of Canine Epidermal Neural Crest Stem Cell Transplantation in the Spinal Cords of Dogs.

Journal

Stem cells translational medicine, 4(10)

ISSN

2157-6564

Authors

McMahill, Barbara G
Spriet, Mathieu
Sisó, Sílvia
et al.

Publication Date

2015-10-01

DOI

10.5966/sctm.2015-0018

Peer reviewed

STEM CELLS TRANSLATIONAL MEDICINE®

PROTOCOLS AND MANUFACTURING FOR CELL-BASED THERAPIES

Feasibility Study of Canine Epidermal Neural Crest Stem Cell Transplantation in the Spinal Cords of Dogs

BARBARA G. MCMAHILL,[a] MATHIEU SPRIET,[b] SÍLVIA SISÓ,[c] MICHAEL D. MANZER,[c] GAELA MITCHELL,[a] JEANNINE MCGEE,[a] TANYA C. GARCIA,[d] DORI L. BORJESSON,[c] MAYA SIEBER-BLUM,[e] JAN A. NOLTA,[a] BEVERLY K. STURGES[b]

Key Words. Adult stem cells • Epidermal neural crest stem cell • Canine epidermal neural crest stem cells • Canine epidermal neural crest stem cell • Dog model • Spinal cord injury

[a]Stem Cell Program, Institute for Regenerative Cures, University of California Davis Medical Center, Sacramento, California, USA; [b]Department of Surgical and Radiological Sciences, [c]Department of Pathology, Microbiology and Immunology, and [d]J.D. Wheat Veterinary Orthopedic Research Laboratory, School of Veterinary Medicine, University of California, Davis, California, USA; [e]Institute of Genetic Medicine, Centre for Life, Newcastle University, Newcastle Upon Tyne, United Kingdom

Correspondence: Beverly K. Sturges, D.V.M., Department of Surgical and Radiological Sciences, School of Veterinary Medicine, University of California Davis, 1402 Tupper Hall, Davis, California 95616, USA. Telephone: 530-752-7545; E-Mail: bksturges@ucdavis.edu

Received February 4, 2015; accepted for publication June 17, 2015; published Online First on August 13, 2015.

1066-5099/2015/$20.00/0

http://dx.doi.org/10.5966/sctm.2015-0018

ABSTRACT

This pilot feasibility study aimed to determine the outcome of canine epidermal neural crest stem cell (cEPI-NCSC) grafts in the normal spinal cords of healthy bred-for-research dogs. This included developing novel protocols for (a) the ex vivo expansion of cEPI-NCSCs, (b) the delivery of cEPI-NCSCs into the spinal cord, and (c) the labeling of the cells and subsequent tracing of the graft in the live animal by magnetic resonance imaging. A total of four million cEPI-NCSCs were injected into the spinal cord divided in two locations. Differences in locomotion at baseline and post-treatment were evaluated by gait analysis and compared with neurological outcome and behavioral exams. Histopathological analyses of the spinal cords and cEPI-NCSC grafts were performed at 3 weeks post-transplantation. Neurological and gait parameters were minimally affected by the stem cell injection. cEPI-NCSCs survived in the canine spinal cord for the entire period of investigation and did not migrate or proliferate. Subsets of cEPI-NCSCs expressed the neural crest stem cell marker Sox10. There was no detectable expression of markers for glial cells or neurons. The tissue reaction to the cell graft was predominantly vascular in addition to a degree of reactive astrogliosis and microglial activation. In the present study, we demonstrated that cEPI-NCSC grafts survive in the spinal cords of healthy dogs without major adverse effects. They persist locally in the normal spinal cord, may promote angiogenesis and tissue remodeling, and elicit a tissue response that may be beneficial in patients with spinal cord injury. STEM CELLS TRANSLATIONAL MEDICINE *2015;4:1173–1186*

SIGNIFICANCE

It has been established that mouse and human epidermal neural crest stem cells are somatic multipotent stem cells with proved innovative potential in a mouse model of spinal cord injury (SCI) offering promise of a valid treatment for SCI. Traumatic SCI is a common neurological problem in dogs with marked similarities, clinically and pathologically, to the syndrome in people. For this reason, dogs provide a readily accessible, clinically realistic, spontaneous model for evaluation of epidermal neural crest stem cells therapeutic intervention. The results of this study are expected to give the baseline data for a future clinical trial in dogs with traumatic SCI.

INTRODUCTION

Spontaneous canine spinal cord injury (SCI) in dogs has been recognized as a valuable animal model that is comparable to human SCI and therefore bridges the gap between rodent studies and human SCI [1–4]. The rationale for our study was based on the rarity of data available on transplantation of somatic stem cells into the healthy spinal cord [5]. Furthermore, epidermal neural crest stem cells (EPI-NCSCs) represent a novel candidate stem cell type for cell-based therapies, but they had not yet been tested in a large-animal model of human disease. Numerous canine experimental studies that evaluate the safety and efficacy of a variety of stem cell interventions have been reported in SCI models [5]. Following translational studies, clinical trials using stem cells for the treatment of canine SCI are now emerging [5]. Notably, the current study is the first report on somatic stem cell grafts in the uninjured spinal cord.

EPI-NCSCs have unique advantages compared to other stem cells used in SCI [6–8]. EPI-NCSCs exist in an easy-to-access location: the hair follicle, and they can be isolated as highly pure populations of multipotent stem cells. EPI-NCSCs can be expanded ex vivo into millions of stem cells in a timely manner, providing numbers sufficient for transplantation [6, 9]. Although allogeneic grafts may be more feasible, autologous transplantation represents an ideal

starting point, because it maximizes the likelihood of successful survival of grafted cells with no need for immunosuppression. EPI-NCSCs have a high degree of plasticity, and they are able to undergo directed differentiation into all major neural crest derivatives and into noncrest cell types [6, 8, 10]. However, it is primarily the close ontologic relationship between neural crest cells and spinal cord progenitor cells in the vertebrate embryo that makes EPI-NCSCs a desirable candidate for SCI [11]. Previous work from the Sieber-Blum laboratory [12, 13] demonstrated that EPI-NCSCs are compatible with the spinal cord environment in two murine models of SCI. It remains to be determined whether EPI-NCSCs from higher vertebrates behave in a similar manner when grafted in the spinal cord. This pilot study was the first step toward determining whether the cells can be labeled ex vivo, safely transplanted into the spinal cords of dogs, and tracked in the live animal without adverse reactions. The current data will facilitate the use of these cells in a naturally occurring model of disease in dogs.

To successfully treat SCI, neural function needs to be improved. The main goals in stem cell transplantation for spinal cord repair include: reconnection of ascending and descending injured axons, likely by alternative pathways, remyelination of demyelinated axons, and secretion of trophic factors to promote an environment conducive to regeneration [14, 15]. When grafted into the contused spinal cords of mice, murine EPI-NCSCs (mEPI-NCSCs) survived in the spinal tissue in large numbers, did not migrate away from the site of injection, and did not form tumors [12]. Cell subsets differentiated into GABAergic neurons, myelin basic protein-positive cells, and myelinating cells. Finally, EPI-NCSCs may secrete trophic factors and promote revascularization [12]. They also produce metalloproteases, a hallmark for neural crest cells, and are thus likely to affect scar formation. Notably, mice that received grafts of mEPI-NCSCs in a contused spinal cord model showed statistically significant improvements in sensory connectivity, as measured by spinal cord-evoked potentials and in touch perception [16].

In this study, we isolated canine EPI-NCSCs (cEPI-NCSCs) from dog hair follicles using a technique that takes advantage of the migratory ability of neural crest cells, avoiding contamination by keratinocytes [8]. After a 10-day ex vivo expansion, we made an autologous transplant of labeled cEPI-NCSCs in the spinal cords of healthy bred-for-research dogs. We tracked the location and persistence of cEPI-NCSCs within the spinal cord and evaluated adverse effects of treatment on the normal spinal cord through subjective and objective measures.

Materials and Methods

Animals

Two 1-year-old bred-for-research beagles (Marshall BioResources, North Rose, NY, https://www.marshallbio.com USA) were included in this study. All animal experiments were performed with ethical approval by the University of California Davis Institutional Animal Care and Use Committee (IACUC) under Protocol 17514. The dogs were euthanized 3 weeks after cEPI-NCSC transplantation. This endpoint was selected to ensure that the grafted cells could be successfully tracked in vivo, and would have time to elicit neurologic and tissue responses, but would also persist in high enough numbers to assess the cells histopathologically at the end of the study.

Bulge Explants, Isolation, and Labeling of cEPI-NCSCs

Haired, full-thickness punch biopsies of the skin were obtained from the dorsum under sedation with dexmedetomidine (5.0 μg/kg i.v.). Canine hair follicles were microdissected as we have described previously [8]. Briefly, the midfollicular area was excised and cut in half, and each piece was placed into a well of a 24-well plate. The explants were incubated in a humidified atmosphere. Three days after onset of emigration, cEPI-NCSCs from the bulge explant were subcultured. At the end of the 5-day-long first subculture, the cells were isolated with TrypLE (Invitrogen, Paisley, U.K., http://www.invitrogen.com; catalog no. 12563) and seeded at 225,000 cells per T225 cm^2 CELLstart-coated (Life Technologies, Rockville, MD, http://www.lifetech.com) culture flask for further ex vivo expansion. On day 3 of expansion in second subculture, cells were predifferentiated into putative neural stem cell-like cells, similar to the protocol we have described previously [8]. The culture medium consisted of NeuroCult NS-A (StemCell Technologies, Vancouver, BC, Canada, http://www.stemcell.com; catalog no. 05750), supplement B27 without retinoic acid (Invitrogen; catalog no. 12587-10), 1% (vol/vol) defined, GMP grade, fetal bovine serum (HyClone, Logan, UT, http://www.hyclone.com; catalog no. SH30070.02), 10 ng/ml recombinant human fibroblast growth factor 2 (rhFGF2) (R&D Systems Inc., Minneapolis, MN, http://www.rndsystems.com; catalog no. 233FB/CF), 20 ng/ml recombinant human epidermal growth factor (rhEGF) (R&D Systems Inc.; catalog no. 236EG/CF), 10 ng/ml recombinant human neurotrophin-3 (rhNT-3) (R&D Systems Inc.; catalog no. 267N3/CF), GlutaMAX (1:100), penicillin/streptomycin (1:100), and 2.5 μg/ml amphotericin B (1:100) [17]. For some experiments, the cells were labeled with NIMT FeOlabel Texas Red (Genovis, Cambridge, MA, http://www.genovis.com; catalog no. F0-FL2-050) following the manufacturer's instructions at the following concentrations: 25 and 50 pg of iron per cell for labeling experiments or 40 pg of iron per cell for injection into the spinal cord. When prepared for injection, the cells were isolated and resuspended at the concentration of 2 million cells per 10 μl of Hanks' balanced salt solution ($-Ca^{2+}$, $-Mg^{2+}$) (Invitrogen; catalog no. 14175-079).

Proliferation and viability experiments were performed to evaluate cEPI-NCSCs after labeling and to determine the optimal iron concentration for in vivo studies. Cells were labeled with NIMT FeOlabel (Genovis; catalog no. F0-FL1-050), as described above. Slides of labeled cells were stained with Perls' Prussian Blue stain for iron identification. Cell proliferation was evaluated by immunocytochemistry using a mouse anti-Ki67 (clone MIB1) antibody (supplemental online Table 1). A commercially available viability assay was used to evaluate cell survival after labeling (Live/Dead Viability/Cytotoxicity Kit; Invitrogen; catalog no. MP03224). Cells were acquired on an FC500 flow cytometer using CXP software (Beckman Coulter, Hialeah, FL, http://www.beckmancoulter.com). The data were analyzed using FlowJo software (Tree Star, Ashland, OR, http://www.treestar.com). A minimum of 100,000 events were collected.

Teratoma Assays

Preliminary safety of the cEPI-NCSCs was determined in an in vivo mouse model to rule out teratoma formation. Rodent work was performed under an approved IACUC protocol in the University of California Davis Stem Cell Program Immunodeficient Mouse Core. Four NOD.Cg-Prkdcscid Il2rgtm1Wjl/SzJ knockout mice were included in the study (two males and two females). Canine EPI-NCSCs were isolated and injected subcutaneously in the left flank at 1×10^6 cells total. The mice were monitored daily for the formation of teratomas. At 3 months, the mice were euthanized and subjected to full

postmortem examination to confirm biosafety [18]. A full review was performed by an anatomic pathologist (B.G.M.).

Spinal Surgery and Transplantation of cEPI-NCSCs

Transplantation of cEPI-NCSCs into the spinal cord was performed 3 weeks after the initial skin biopsy. Under general anesthesia, a routine surgical approach was made to the thoracolumbar vertebral column, and left-sided hemilaminectomies were performed at T12-T13 and L2-L3. Epidural fat was removed to expose the dura mater on the lateral aspect of the spinal cord. cEPI-NCSCs were transplanted using a 25-μl microsyringe (Hamilton Co., Reno, NV, http://www.hamiltoncompany.com) with a 26-gauge needle mounted on a stereotactic frame (Kopf Instruments, Tujunga, CA, http://www.kopfinstruments.com). Each injection contained 2×10^6 autologous cEPI-NCSCs resuspended in 10 μl of Hanks' balanced salt solution. A 0.5-mm-long meningeal incision was performed with a scalpel, which allowed the needle to be slowly introduced into the lateral aspect of the spinal cord without cord deformation to a depth of 2.5 mm below the dura. cEPI-NCSCs were delivered by slow infusion into the white matter of the left lateral funiculus at the level of L2 and L3 spinal cord segments over 5 minutes. Placebo infusions were performed similarly at T12 and T13 spinal cord segments by delivering equal volumes of Hanks' balanced salt solution. Each infusion was performed over 5 minutes at the rate of 2 μl/minute using a microsyringe pump controller (Micro4; catalog no. IM062403; World Precision Instruments, Inc., Sarasota, FL, http://www.wpiinc.com). To minimize evacuation of the inoculum via the needle tract, the needle was left in place for 2 minutes following completion of the injection. The needle was then slowly removed (0.5 mm/minute), and the dural incision was covered with a 0.2-mm piece of gel foam (absorbable gelatin sponge; Pfizer, New York, NY, http://www.pfizer.com).

Clinical Features, Behavioral Assessment, and Gait Analysis

Physical and neurological examinations were performed prior to surgery, daily for 7 days postsurgery, and weekly for the remainder of the study by a board-certified veterinary neurologist (B.K.S.). Behavioral (subjective) assessment was performed through observation and examination to evaluate the impact of cEPI-NCSCs on pelvic limb function. Dogs were videotaped and scored using the Olby functional scoring system [19] before surgery and 1 and 3 weeks after surgery (B.K.S.). In addition, objective gait analysis was performed before surgery to establish each dog's normal baseline and again at week 3 postsurgery to determine any subtle gait alterations secondary to SCI that might be created by the implantation of cells but that might not be ascertained by behavioral analysis alone. Kinetic and kinematic parameters were obtained from each gaiting session. In brief, dogs were led at a trot by an experienced handler at speeds that were comfortable to the dog. The dogs traversed a 6-m-long walkway that contained 2 embedded 60 $\times$ 40-cm force plates in series. Five IR beam-timing gates along the walkway at 0.5-m spacing were used to trigger software to determine dog velocity and acceleration (mean value over 5 m). Four to six trials were recorded at a trot (1.41–2.06 m/second). Gait trials were considered valid if dog acceleration was within $\pm$0.5 m/second^2 for the duration of the trial, fore limb paw strikes were recorded on the force platforms, and dogs traveled in a straight line without pulling on the leash. For capturing limb motion, spherical reflective markers were taped to the fur or skin at defined anatomical landmarks (supplemental online Fig. 1). Latero-lateral motion of the pelvis and thorax in the horizontal plane were also measured using markers (supplemental online Fig. 1). Range of motion (ROM) was calculated for limb joint angles as the difference between maximum and minimum joint angle during a gait cycle. ROM of the midillial (pelvis) and midscapular (thorax) markers were calculated and expressed as the difference between maximum and minimum medio-lateral displacement in the horizontal plane. Weight bearing was measured as vertical and cranio-caudal maximum ground reaction forces (GRF) normalized as a percentage of body weight. Symmetry in the vertical GRF between the right and left limbs was analyzed using the using the following asymmetry index =($|XR - XL|/[|XR + XL| \times 0.5]) \times 100$ [20]. The effects of limb (left, right) on all variables were assessed using a mixed model analysis of variance. Statistical models included the effects of limb (left, right), dog speed and repeated measures within each dog. To evaluate the effect of treatment, statistical analyses were performed, and post hoc comparisons were made by estimating least-squares means including both dogs adjusted for the other factors in the model with a level of significance of $p < .05$.

Cerebrospinal Fluid Analysis

Cerebrospinal fluid (CSF) was routinely collected at the cisterna magna 2 weeks prior to cEPI-NCSC transplantation, 2 days following cell transplantation, and once again immediately prior to euthanasia. Two milliliters of CSF were collected by free flow and submitted to the clinical laboratory at the William R. Pritchard Veterinary Medical Teaching Hospital for analysis. Analyses included a total cell count and differential, determination of protein concentration, and a complete cytologic review by a board-certified veterinary clinical pathologist (D.L.B.).

Magnetic Resonance Imaging

Dogs were imaged using a 1.5T magnetic resonance imaging (MRI) unit (GE Signa HDxt; General Electric, Milwaukee, WI, http://www3.gehealthcare.com/en). To determine ideal FeO-label concentration for MRI tracking, labeled cEPI-NCSCs were injected into the spinal cords of cadaver dogs. In the thoracolumbar region, the following 10-μl injections were made: T12 positive control consisting of air; T13 of 3×10^5 cEPI-NCSCs labeled with 25 pg of iron per cell; L1 injection of 3×10^5 cEPI-NCSCs labeled with 50 pg of iron per cell; and L2 negative control consisting of unlabeled cEPI-NCSCs.

For the in vivo tracking study, dogs were imaged before surgery, immediately after surgery and 2 days and 1, 2, and 3 weeks after stem cell administration. MRI was used for cell localization and subjective evaluation of the persistence. No attempt at quantifying cell persistence was made. The dogs were placed under general anesthesia in dorsal recumbency, and the thoracolumbar spine was imaged from the 11th thoracic vertebra to the 4th lumbar vertebra using a dedicated spine coil. Transverse and sagittal images were acquired using T2-weighted fast spin echo (T2 FSE) and multiple echo recombined gradient echo (MERGE) sequences. Transverse images were also obtained using a three-dimensional spoiled gradient echo (SPGR) sequence. Images were assessed for signal void because of a susceptibility artifact from the iron oxide label associated with the stem cells. Other signal changes in the spinal cord parenchyma

were also evaluated. The review was performed by a board-certified veterinary radiologist (M.S.).

Histopathology and Immunohistochemistry

The 2 dogs were euthanized 3 weeks after surgery, and complete postmortem examinations were performed. A full review was performed by a board-certified veterinary anatomic pathologist (B.G.M.) and a neuropathologist (S.S.). The spinal cords were immediately harvested. Tissues were fixed for 24 hours to 5 days in 10% neutral buffered formalin. Formalin-fixed tissue was embedded in paraffin, and 5-μm-thick sections were stained with H&E. Special stains were performed for evaluation of collagen and iron depositions: Masson's trichrome and Perls' Prussian Blue, respectively. Demyelination was evaluated by a combined H&E and Luxol fast blue stain.

For immunohistochemistry, 4-μm-thick sections were deparaffinized and rehydrated. Depending on the specific requirements for each immunohistochemistry, antigen retrieval included either heat-induced epitope retrieval, enzymatic digestion, or no retrieval. The antibody diluent was phosphate-buffered saline-Tween 20 (0.02%), and the blocking reagent was 10% normal horse serum.

A panel of 15 antibodies that recognize the corresponding canine protein was used (a) to evaluate cEPI-NCSCs (rabbit anti-nestin, goat anti-Sox10, mouse anti-βIII-tubulin, mouse anti-synaptophysin, mouse anti-myelin basic protein, mouse anti-microphthalmia, and mouse anti-Ki67), (b) to assess changes in vasculature (mouse anti-smooth muscle actin, rabbit anti-factor VIII, mouse anti-CD31, mouse anti-vimentin, and rabbit anti-laminin), (c) to assess glial reaction (rabbit anti-glial fibrillary acidic protein and mouse anti-CD18), and (d) to study the inflammatory response (mouse anti-CD18 and rat anti-CD3). The primary antibody was applied and incubated for 1 hour in a humidity chamber at room temperature.

Depending on antigen requirements, detection was performed by using either Dako Envision System-horseradish peroxidase (HRP) (mouse K4001 and rabbit K4003) or Biocare Medical 4Plus Detection System (mouse link HM606, rabbit link GR608, rat link GR607, and goat link MG610H) (supplemental online Table 1). Biocare Medical streptavidin-HRP (HP604) was applied to label the Biocare links. Finally, all labels were visualized with NovaRed for peroxidase (Vector SK-4800), per the manufacturer's instructions. Sections were counterstained in Mayer's hematoxylin. Intracellular iron oxide in cEPI-NCSCs was detected by Prussian Blue staining.

Positive controls were selected based on tissue specificity of expression for each marker (supplemental online Table 1). Negative controls consisted of substitution of primary antibody with an isotype-matched irrelevant IgG.

Results

Bulge Explants, Isolation, and Labeling of cEPI-NCSCs

Similar to data we have reported previously, cEPI-NCSCs emerged from hair follicular explants within 6 days after explantation, and they migrated and proliferated rapidly [8–10]. An ex vivo expansion was subsequently performed for 10 days to achieve numbers suitable for transplantation. An average of 3.5 million cells were obtained per hair follicle within 8 days [8]. We have shown previously in compound transgenic mice that all emigrating cells are of neural crest origin and that the majority of them are multipotent, self-renewing stem cells [9]. We obtained comparable results with cEPI-NCSCs [8].

Cells were labeled with iron oxide particles for 24 hours to assess any effect of iron oxide on early cell viability. cEPI-NCSCs survived and continued to proliferate ex vivo (Fig. 1A–1C) after labeling. At a concentration of 25 pg of iron oxide particles per cell, 34% $\pm$ 16% of cells contained iron, whereas at 50 pg of iron per cell, 70% $\pm$ 10% of cells contained iron (Fig. 1A′, 1B′, 1C′). Cells for grafts were labeled with 40 pg of iron oxide particles per cell. The proliferation marker Ki67 was expressed in the nucleus of 59% $\pm$ 37% cells at 25 pg of iron oxide particles per cell and in 78% $\pm$ 41% of cells at 50 pg of iron oxide particles per cell (Fig. 1A′′, 1B′′, 1C′′). At the end of the 24-hour labeling period, 98% of cells labeled with 25 pg of iron were viable, and 98% of the cells labeled with 50 pg of iron oxide particles were viable (Fig. 1B′′′, 1C′′′). This viability was exactly the same as for unlabeled cells (98%) (Fig. 1A′′′).

Teratoma Assays

At the end of the 3-month observation period, full post-mortem exams were performed on the 4 mice injected with stem cells. The tissues examined histologically include serial sections at the injection site (haired skin, subcutaneous tissue, and adjacent skeletal muscle), stomach, small intestine, large intestine, pancreas, liver, spleen, lungs, heart, adrenals, and kidneys. All tissues were within normal limits. There was no tumor formation or tissue reaction at the injection site or at any remote sites. cEPI-NCSCs were not observed at the injection site or remote sites. In teratoma assays, nonformation of teratomas by the test cells is an indication that the cells are not tumorigenic [18, 21].

Clinical Features, Behavioral Assessment, and Gait Analysis

Neurological examinations performed prior to surgery were within normal limits. Immediately following surgery, both dogs were fully ambulatory but had subtly decreased conscious proprioception (based on neurological exam) in both pelvic limbs, worse on the left side. By postoperative days 3 (dog 2) and 5 (dog 1), the neurological examination was returned to original baseline, that is, within normal limits. In both dogs, functional scoring (Olby score) indicated normal pelvic limb gait at presurgical baseline and at 7 days and 21 days postsurgery. Although the dogs received routine opioid analgesia following stem cell transplantation in the immediate postoperative period, the dogs did not exhibit signs of overt pain thereafter and were treated with oral pain medication Ultram (tramadol hydrochloride, 50 mg; Amneal Pharmaceuticals, Bridgewater, New Jersey, http://amneal.com) and the nonsteroidal anti-inflammatory drug Metacam (meloxicam, 1.5 mg/ml oral suspension; Boehringer Ingelheim GmbH, Ingelheim, Germany, http://www.boehringer-ingelheim.com) for a period of 5 days following surgery.

In the evaluation of objective gait measures, mean gait parameters of both dogs combined were compared pretransplantation to 21 days post-transplantation of stem cells into the spinal cord (Table 1). In the fore limbs, the mean carpal ROM (°) decreased significantly ($p < .05$) by 18%, the maximum vertical GRF (percentage of body weight) decreased 4%, the stance duration (percentage of gait cycle) decreased 4%, and the swing duration increased 6%. In the hind limbs, stifle ROM increased significantly by 13%, and hip ROM decreased by 16%. The maximum vertical GRF in the hind limbs did not change significantly, but the stance duration decreased by 9%, and swing duration

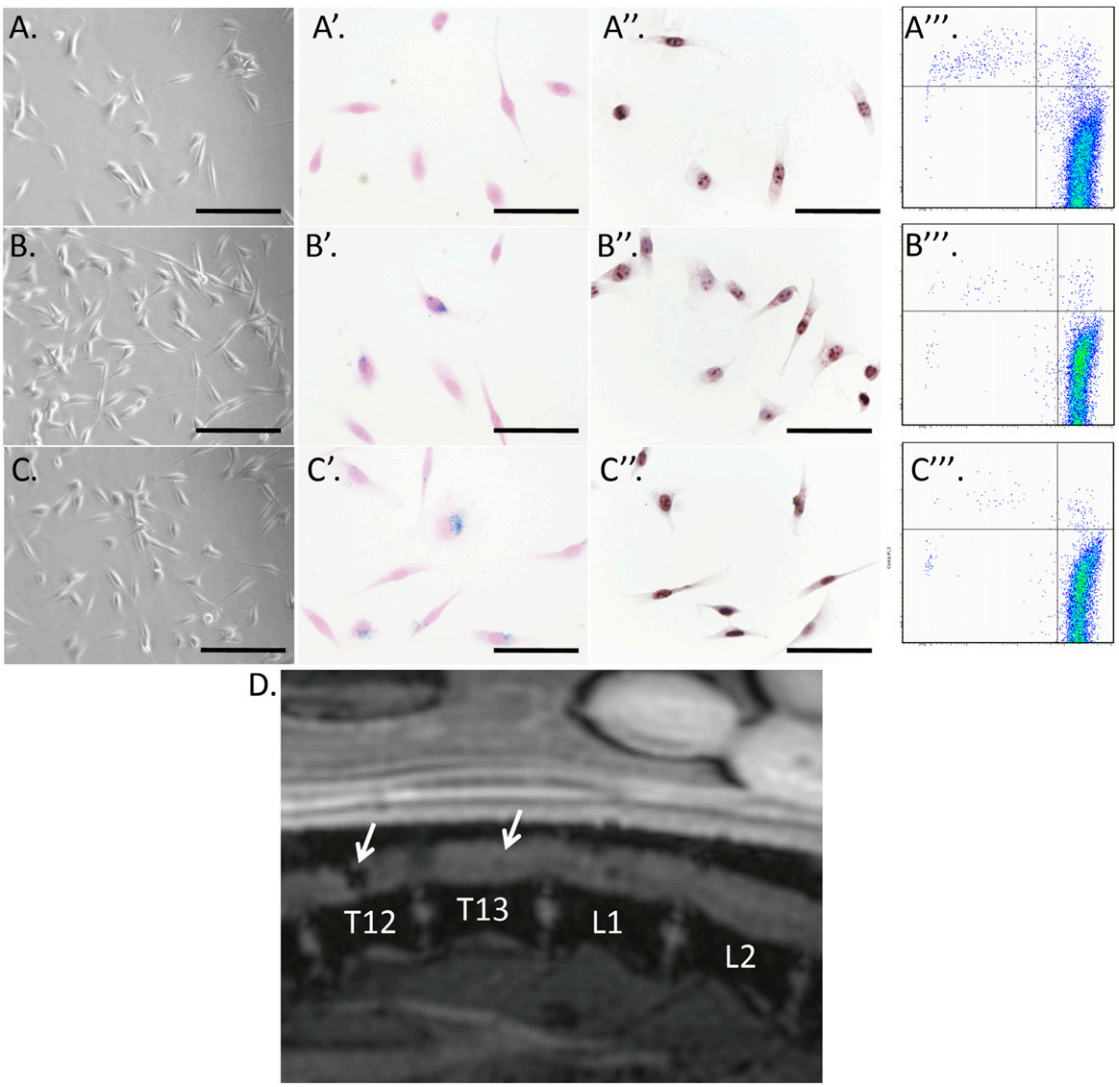

Figure 1. Labeling of epidermal neural crest stem cells (EPI-NCSCs) with NIMT FeOlabel. **(A):** Unlabeled canine EPI-NCSCs (cEPI-NCSCs) after ex vivo expansion (phase contrast). Scale bar = 100 μm. **(A′):** Iron is not observed in any cEPI-NCSCs (Prussian Blue). Scale bar = 50 μm. **(A″):** Immunocytochemistry for the proliferation marker Ki67, with 90.07% $\pm$ 13.18% of cells proliferating. Scale bar = 50 μm. **(A‴):** Viability assessment shows survival of 97.58% of cEPI-NCSCs. **(B):** cEPI-NCSCs after ex vivo expansion, 24 hours after iron labeling with 25 pg of iron per cell, phase contrast. Scale bar = 100 μm. **(B′):** At this concentration of iron, 34.20% $\pm$ 16.29% of cells contain iron within the cytoplasm (Prussian Blue). Scale bar = 50 μm. **(B″):** Immunocytochemistry for the proliferation marker Ki67, with 58.64% $\pm$ 37.20% of cells proliferating. Scale bar = 50 μm. **(B‴):** Viability assessment shows cEPI-NCSC survival of 97.86%. **(C):** cEPI-NCSCs labeled with 50 pg of iron per cell, phase contrast. Scale bar = 100 μm. **(C′):** At 50 pg of iron per cell, 69.84% $\pm$ 9.92% of cells contain iron within the cytoplasm (Prussian Blue). Scale bar = 50 μm. **(C″):** Immunocytochemistry for the proliferation marker Ki67, with 77.50% $\pm$ 41.04% of cells proliferating. Scale bar = 50 μm. **(C‴):** Viability assessment shows cEPI-NCSC survival of 98.04%. **(D):** Sagittal gradient echo T2$*$ magnetic resonance image of a spinal cord from T12 to L2. A T12 positive control site with injection of 10 μl of air is shown. As expected, an area of signal void is identified (arrow). With T13 injection of 3×10^5 cEPI-NCSCs labeled with 25 pg of iron per cell, a small hypointense area is identified in the spinal parenchyma at the site of injection (arrow). With L1 injection of 3×10^5 cEPI-NCSCs labeled with 50 pg of iron per cell, the hypointense area at the site of injection is better defined and larger than at T13. With L2 negative control (unlabeled cEPI-NCSCs), no abnormalities were observed in the spinal cord.

increased by 5%. The asymmetry index did not change in fore limbs or hind limbs, and there was no significant difference in the left-to-right range of motion of the thorax and pelvis in the horizontal plane following transplantation of stem cells.

Cerebrospinal Fluid Analysis

The CSF fluid from both dogs was cytologically similar throughout the study. Before cell transplantation, the CSF fluid was normal (total cell count, $<$3 cells per microliter; protein concentration, $<$25 mg/dl). Two days after surgery (laminectomy and cell transplantation), the CSF cell count was markedly increased in both dogs (70 and 177 cells per microliter) secondary to a moderate neutrophilic inflammation. There was also some cytologic evidence of lymphocyte reactivity and mild hemorrhage. Three weeks after cell transplantation (immediately before euthanasia), the CSF had mostly returned to normal with a normal total cell count (1 and 4 cells per microliter) and a mild increase in protein

Table 1. Gait analysis kinetic and kinematic parameters

Parameters	Pre-Tx	Post-Tx	*p* value
Fore limbs			
Carpus ROM (°)	119.4 ± 15.7	98.1 ± 12.1	**<.0001**
Elbow ROM (°)	66.6 ± 6.4	68.2 ± 9.8	.127
Shoulder ROM (°)	24.6 ± 4.0	26.2 ± 7.3	.262
Maximum vertical GRF (% BW)	52.8 ± 4.1	50.8 ± 5.1	**.000**
Maximum cranial GRF (braking force, % BW)	7.7 ± 2.2	7.4 ± 1.8	.133
Maximum caudal GRF (propulsive force, % BW)	−4.3 ± 1.0	−3.9 ± 1.6	.148
Stance duration (% gait cycle)	43.5 ± 2.3	40.1 ± 3.5	**.001**
Swing duration (% gait cycle)	56.2 ± 2.3	59.9 ± 3.5	**.000**
Asymmetry index vertical GRF (%)	4.9 ± 4.8	7.1 ± 4.8	.478
Hind limbs			
Hock ROM (°)	52.9 ± 8.9	56.6 ± 13.8	.086
Stifle ROM (°)	55.6 ± 3.7	62.6 ± 5.0	**<.0001**
Hip ROM (°)	34.3 ± 5.4	28.7 ± 8.5	**<.0001**
Maximum vertical GRF (% BW)	34.2 ± 3.7	35.5 ± 5.7	.995
Maximum cranial GRF (braking force, % BW)	1.3 ± 1.1	1.6 ± 1.1	.326
Maximum caudal GRF (propulsive force, % BW)	−4.5 ± 1.3	−4.4 ± 1.3	.608
Stance duration (% gait cycle)	32.5 ± 2.4	29.5 ± 2.8	**.001**
Swing duration (% gait cycle)	67.5 ± 2.4	70.5 ± 2.8	**.001**
Asymmetry index vertical GRF (%)	8.1 ± 6.8	8.1 ± 6.3	.730
Thorax/pelvis sway			
ROM mid-ilium latero-lateral motion [44]	0.038 ± 0.017	0.033 ± 0.014	.170
ROM mid-scapula latero-lateral motion (m)	0.027 ± 0.014	0.029 ± 0.012	.772

Shown are average values of both dogs for fore limbs, hind limbs, and thorax/pelvis anatomical landmarks (means ± SD). Bold values indicate parameters that reached significance at the $p < .05$ level.
Abbreviations: BW, body weight; GRF, ground reaction forces; Pre-Tx, pretreatment; Post-Tx, post-treatment; ROM, range of motion.

concentration in dog 2 (24 and 40 mg/dl). Dog 1 had a mild increase in eosinophils and lymphocytic reactivity that was not present in dog 2.

Magnetic Resonance Imaging

Based on the cEPI-NCSC labeling experiment, the optimized concentration of iron was determined to be 40 pg of iron per cell (Fig. 1). On MRI, iron oxide is expected to be visible as an area of signal void, which could be observed with concentrations as low as 25 pg of iron oxide per cell and as high as 50 pg of iron oxide per cell (Fig. 1D). The higher concentration provided better conspicuity of the site of injection. Unlabeled cEPI-NCSCs were not visible on MRI.

No signal void could be observed in the spinal cord parenchyma at the T12 and T13 injection sites at any time point in both dogs. Mild intraparenchymal T2 hyperintensity was present after injection at these sites but was resolved by week 1. A large area of signal void, centered on the left side of the spinal cord and covering more than 50% of the spinal parenchyma on the MERGE sequence was present at the L2 and L3 injection sites of dog 1 and at the L2 injection site of dog 2 immediately after injection (Fig. 2A, 2B). This signal void was also observed on the SPGR sequence, in which it appears smaller than on the MERGE sequence. This signal void persisted up to 3 weeks after injection. A slight reduction in size of the area of signal void was observed on dog 1. A more substantial size reduction was present in dog 2. At the L3 injection site of dog 2, the signal void was epidural at the day of injection and regressed in size on subsequent images (Fig. 2B). A focal hypointense signal was present on T2 weighted images in the spinal cord at the L2 and L3 sites of dog 1 and at the L2 site of dog 2, corresponding to the signal void observed in the gradient echo sequences but covering a smaller area. A rim of T2 hyperintensity was present surrounding the hypointense area at day 2 after injection but regressed over time.

Correlation Between MRI and Pathology at Injection Sites

At week 3, it was still possible to detect cEPI-NCSCs because of the susceptibility artifact from the iron oxide in the spinal cords of both dogs by MRI (Fig. 3A–3D). Side by side comparison between MRI sequences and gross pathology emphasizes that, as expected, this labeling technique is not suitable for quantification because the size of the artifact is dependent on the type of MRI sequence used and because it covers an area much larger than the actual area of distribution of iron oxide particles in the tissue (Fig. 3B, 3B′, 3D, 3D′). On gross pathology, at the L2 graft site, brown iron pigment contrasted with white spinal cord parenchyma, providing simple visual location of the implant on the left side on the dorsal lateral funiculi (Fig. 3B′, 3D′). Also, a rim of tissue reactivity was present around the iron oxide label. No changes were noted grossly on control injections (Fig. 3A′, 3C′). From the center toward the periphery, implants were composed of labeled cEPI-NCSCs, vascular reaction, cellular reaction, and tissue damage (Fig. 3B′′, 3B′′′, 3D′′, 3D′′′). In the center of the graft, a few apoptotic cells, defined by nuclear morphology, were observed in both dogs. To evaluate the extent of tissue damage, representative sections of cervical, thoracic, and the entire lumbar spinal cord were examined histologically. The damage extended less than 350 μm rostral and caudal from the injection site. Tissue damage was observed in both sham injections and cEPI-NCSC injections and was characterized by myelin loss, spheroid formation, and Wallerian-like axonal degeneration (Fig. 3C′, 3F′). In all examined sections, resident neurons in the gray matter were within normal limits.

Characterization of cEPI-NCSC Implants and Surrounding Spinal Cord Tissue Reaction

In tissue sections, grafted cEPI-NCSCs were readily identified by the iron label in the left lateral funiculi of the spinal cord at L2 3 weeks postinjection (Fig. 4A, 4B). The exclusive location of iron oxide within cEPI-NCSCs was confirmed by lack of coexpression of CD18, a panleukocyte/macrophage marker. Large numbers of cEPI-NCSCs survived in the spinal parenchyma, and they were

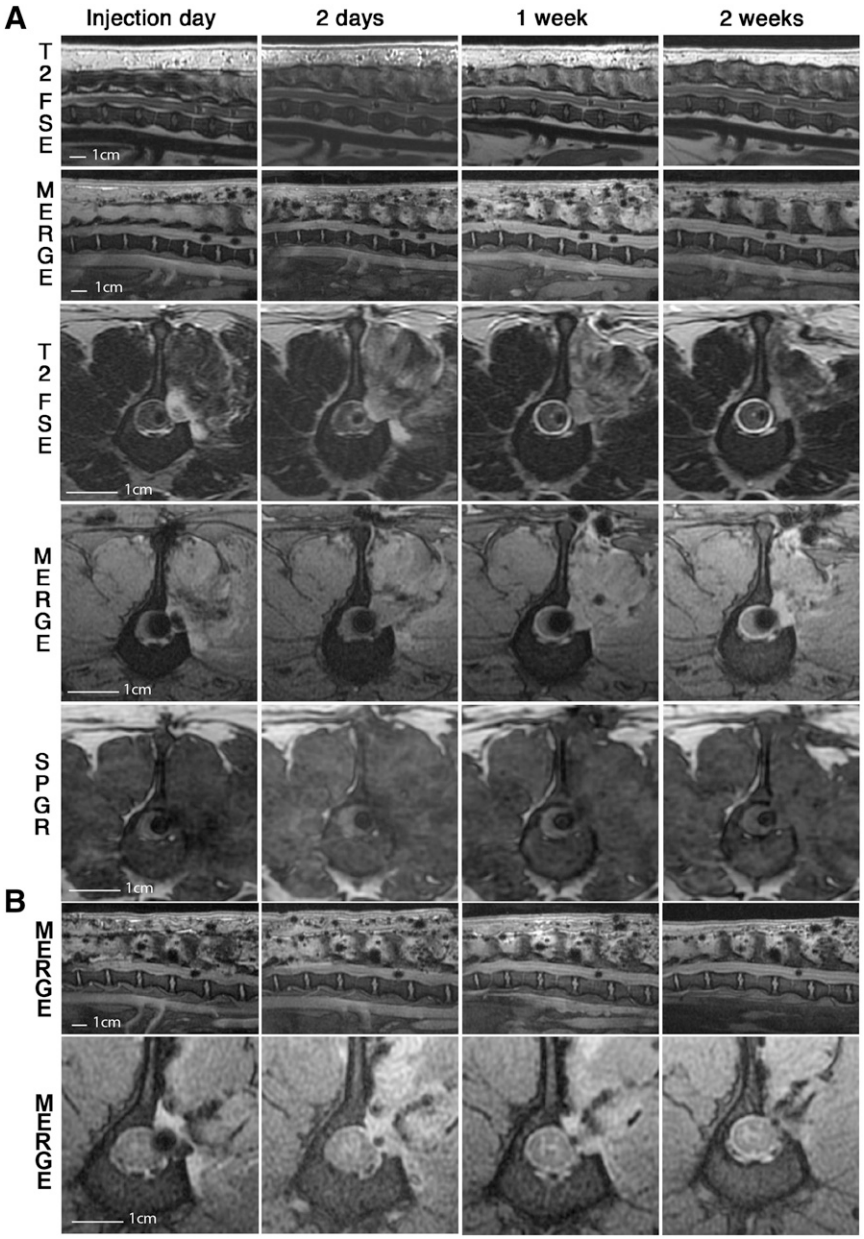

Figure 2. Magnetic resonance sequences. **(A):** Sagittal and transverse images of the spinal cord of beagle 1 in the thoracolumbar area using three different magnetic resonance pulse sequences (T2 FSE, MERGE, and SPGR). Injection of 2×10^6 canine epidermal neural crest stem cells (cEPI-NCSCs) was performed in the spinal cord parenchyma both at L2 and L3. A signal void (hypointense area) caused by a susceptibility artifact created by the iron oxide is identified on all sequences centered on the left side of the spinal cord parenchyma. The signal void is maintained throughout the 2 weeks. The hypointense area is largest on the MERGE images and smallest on the T2 FSE images. The transverse T2 FSE image shows a hyperintense halo surrounding the hypointense signal caused by the presence of the iron oxide-labeled cells. This is most evident at 2 days postinjection and decreases at weeks 1 and 2. **(B):** Sagittal and transverse MERGE images of the thoracolumbar spine of beagle 2. Injection of 2×10^6 cEPI-NCSCs was performed in the spinal cord parenchyma both at L2 and L3 (sagittal images). The signal void at L3 is centered in the peridural space, revealing an inappropriate injection (transverse images). The signal void is regressing faster at the site of the peridural injection when compared with the intraparenchymal injection. Transverse images were also obtained using a three-dimensional spoiled gradient echo sequence. Abbreviations: MERGE, multiple echo recombined gradient echo; SPGR, spoiled gradient echo; T2 FSE, T2-weighted fast spin echo.

intimately associated with numerous discrete reactive blood vessels (Fig. 4C–4H). As shown on the subgross spinal cord microphotographs, most collagen deposition located in the implant corresponded to reactive vascular structures (Fig. 4C′, 4D′). In contrast, control injections showed minimal to absent intraparenchymal collagen deposition or reactive blood vessels (Fig. 4C, 4D). To further evaluate vascular structures such as endothelial cells and basal lamina, the protein expression of factor VIII and laminin was studied, respectively. In the tissues of both dogs, reactive vessels were haphazardly arranged, extending from meninges into the gray matter and traversing the spinal cord in different directions (Fig. 4E, 4F). Expression of laminin in dog 1 was, as expected, associated with reactive vessels within the implant (Fig. 4G′, 4G′′), whereas in dog 2, interestingly, laminin was

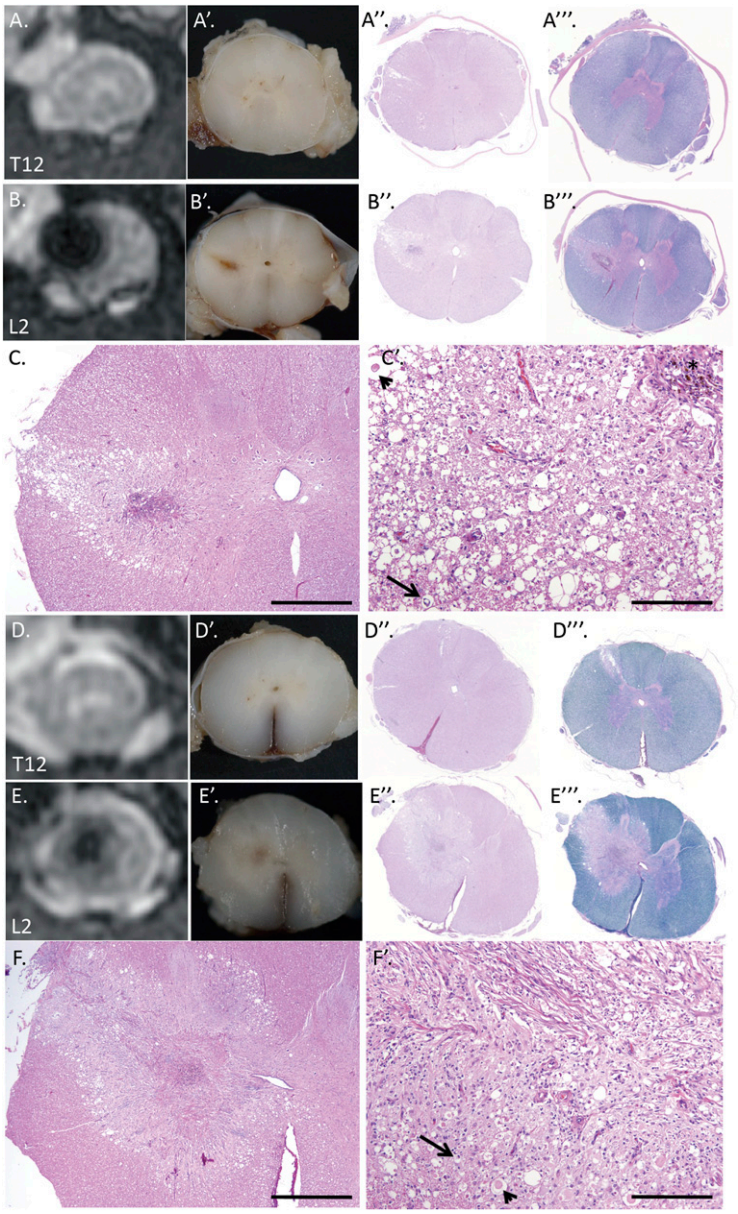

Figure 3. Correlation between magnetic resonance imaging and pathology at injection sites. **(A–C):** Beagle 1 at week 3. **(A):** Control injection at T12, transverse multiple echo recombined gradient echo (MERGE) image, with no signal abnormality in the spinal cord parenchyma. **(A′):** Gross cross-section of T12 spinal cord within normal limits. **(A″):** Control at T12. Note focal demyelination of the white matter and dura thickening resulting from the phosphate-buffered saline (PBS) injection on the left side (H&E). **(A‴):** Control at T12, focal demyelination evident with loss of blue staining, Luxol fast blue, H&E. **(B):** canine epidermal neural crest stem cell (cEPI-NCSC) graft at L2, transverse MERGE image. The hypointense iron signal is persistent at week 3. **(B′):** Gross cross-section of L2 spinal cord. Note on the left side that the cEPI-NCSC graft is readily observed as cells are labeled brown (iron), which contrasts with the white spinal cord. **(B″):** cEPI-NCSC graft at L2. A central cluster of iron-labeled cells is surrounded by tissue reaction and focal demyelination (H&E). **(B‴):** cEPI-NCSC graft at L2. The architecture of the graft is better appreciated (Luxol fast blue, H&E). **(C):** Closer view of **(B″)**. Scale bar = 1 mm. **(C′):** Closer view of **(C)**. Scale bar = 200 μm. Note implanted cells (*) on the top right. From the center to the periphery: cEPI-NCSCs, vascular reaction, astrocytosis/microgliosis, and demyelination. At the periphery of the graft there is spheroid formation (arrowhead) and Wallerian-like degeneration (arrow). **(D–F):** Beagle 2 at week 3. **(D):** Control injection at T12, transverse MERGE image. There is no signal abnormality in the spinal cord parenchyma. **(D′):** Gross cross-section of T12 spinal cord within normal limits. **(D″):** Control at T12, left dorsal lateral funiculi focal demyelination resulting from the PBS injection on the left side, H&E. **(D‴):** Control at T12, focal demyelination evident with loss of blue staining, Luxol fast blue, H&E. **(E):** cEPI-NCSC graft at L2, transverse MERGE image. The hypointense iron signal is persistent at week 3. **(E′):** Gross cross-section of L2 spinal cord. Note on the left side the cEPI-NCSC graft in a more central location than **(B′)**. **(E″):** cEPI-NCSC graft at L2. A central cluster of iron-labeled cells is surrounded by robust tissue reaction and discrete demyelination (H&E). **(E‴):** cEPI-NCSC graft at L2. Myelin loss affects most of the left dorsolateral funiculi (Luxol fast blue, H&E). **(F):** Closer view of **(E″)**. Scale bar = 1 mm. **(F′):** Closer view of **(F)**. Scale bar = 200 μm. From the center to the periphery: cEPI-NCSCs, fibrovascular reaction, astrogliosis and microgliosis, and demyelination. At the periphery of the graft there is spheroid formation (arrowhead) and Wallerian-like axonal degeneration (arrow).

additionally being expressed by numerous spindle-shaped cells intermixed with vascular structures (Fig. 4H′, H′′). The spindle-shaped cells were iron- and Sox10-negative; therefore the fibrovascular reaction was interpreted as granulation tissue. At 3 weeks postgrafting, implants showed a high degree of cohesion. Notably, cEPI-NCSCs remained at the site of injection. No cEPI-NCSCs were observed that translocated to other locations both within and outside the spinal cord.

Differentiation of cEPI-NCSCs in the implant was monitored with a panel of cell type-specific antibodies recognizing cells of interest (neurons and glia), as well as other markers of major neural crest derivatives (myofibroblasts and melanocytes). The only marker being expressed on implanted cEPI-NCSCs 3 weeks postgrafting was the neural crest and Schwann cell marker, Sox10 (Fig. 5A′, 5C′). All other tested markers were not expressed (Table 2). Importantly, no proliferation of cEPI-NCSCs in the spinal cord was observed (Fig. 5A′′, 5C′′). Proliferation marker Ki67 was not expressed in the transplanted cells but was noted in a few lymphocytes that were present within the implant (Fig. 5A′′, 5C′′).

Cellular reaction at the implant site was predominantly characterized by large numbers of hypertrophic astrocytes and macrophages/microglial cells and was more intense in dog 2 (Fig. 5B, 5B′, 5D, 5D′). Inflammatory cells were rarely observed in sham injection sites. An inflammatory reaction composed mainly of a few lymphocytes and gitter cells was minimal in dog 1 (Fig. 5B′′) to mild in dog 2 (Fig. 5C′′, 5D′′). In addition, in the implant of dog 2, a cluster of foreign type multinucleated giant cells was present adjacent to the transplanted cells (Fig. 5D′′).

Discussion

Here we describe the results of a feasibility study essential for future research into cell-based therapy using cEPI-NCSCs. The use of a large-animal model is an important step, because it is well documented that results obtained in rodents are not always representative of the human condition. EPI-NCSCs hold promise in SCI therapy primarily because of their close ontological relationship with spinal cord progenitor cells, because neural crest stem cells and spinal cord stem cells share a common higher order stem cell [11]. Furthermore, in the mouse, murine EPI-NCSCs integrate in the spinal parenchyma without proliferating or migrating, produce diffusible factors that may promote regeneration, and modulate scar formation, and subsets of grafted cells differentiate into neurons and glial cells. All these features make EPI-NCSCs unique candidates for future cell-based therapies in SCI [7, 12]. It was thus essential to test EPI-NCSCs in the dog, an accepted model of human SCI [2, 3, 22]. Similar to EPI-NCSCs from humans and mice, EPI-NCSCs exist in the canine hair follicle, and they share a similar molecular signature with EPI-NCSCs from humans [8–10].

Teratoma assays are used for biosafety analysis to evaluate tumorigenic potential of pluripotent stem cell-derived progeny [18, 23]. Long-term tumorigenic studies in dogs are not feasible given their long life span. In this study, teratoma assays were performed as a first safety analysis for the use of cEPI-NCSCs in future clinical applications. cEPI-NCSCs did not form teratomas. Likewise, mouse EPI-NCSCs did not form tumors when grafted into the spinal cords of syngeneic wild type mice [12, 13, 16]. Overall, we conclude that the absence of teratoma formation by EPI-NCSCs is an indication that the cells are not tumorigenic. Because cEPI-NCSCs are multipotent and not pluripotent cells [8], we hypothesize that upon engraftment, cEPI-NCSCs do not survive and likely die by apoptosis during the course of the teratoma test. For that reason, cEPI-NCSCs were not observed at the injection site or remote sites.

The ideal method to deliver stem cells to the spinal cord remains controversial [24]. Direct delivery into the spinal cord may lead to superior engraftment of delivered stem cells with lower cell losses than other methods. However, the potentially injurious effects of delivering fluid volume into the spinal cord need to be considered carefully because the method of delivery in and of itself may cause injury to the spinal cord.

To further assess changes in functionality that were potentially undetectable on behavioral (neurologic exam and Olby scoring) examination, we used objective gait analysis to determine whether dogs showed any postgrafting changes in various gait parameters. We observed a reduction of carpal joint angle ROM and a decrease in fore limb stance duration greater than the variation seen intertrial and between individuals in normal mixed-breed dogs [25, 26], indicating that the changes may be clinically relevant. The change caused by treatment in the fore limb maximum vertical GRF (4% difference) was similar to the interweek (4.59%) variation in the maximum vertical GRF of normal dogs [27]. In a quadruped, these functional modifications could represent compensatory changes in the fore limbs if hind limb motion was affected by cell transplantation directly or secondary to changes in muscles and ligaments of the dog's axial skeleton caused by extensive dissection of epaxial/hypaxial musculature and supporting elements during the procedure. A previous study in dogs investigated the effect of orthopedic disease on kinematics and kinetics in the hind limbs [28]. Here, dogs with cranial cruciate ligament disease showed that 6° of difference in stifle angle ROM and 4° of difference of hip ROM were not significant compared with normal dogs [28]. Additionally, a difference of 4 (percentage of gait cycle) in stance duration was not a significant difference comparing normal dogs with those with cruciate ligament disease. In our study, the difference was 7 in stifle angle ROM, more than 5 in hip angle ROM, and slightly greater than 3 (percentage of gait cycle) in stance duration. Some observations in the pelvic limb kinematics were similar to affects of orthopedic limb disease. However, other changes were within the variability seen in normal dogs. Because there is no literature on the effects of neurologic disease on kinetic/kinematic outcomes in dogs, it is not known what the exact changes found in the present study represent: effects on musculoskeletal structures, spinal cord injury, or simply discomfort and/or muscular effects from recently performed extensive surgical procedure. Asymmetry indices of both fore limbs and hind limbs indicated a low probability of being lame [27], meaning that weight bearing was not altered preferentially to either side after treatment. This suggests there was not an effect on the spinal cord and peripheral nerves unilaterally as might be expected with unilateral transplants.

Within the body of literature on experimental treatment of SCI using transplantation of stem cells into the spinal cord, the effects of further injury to spinal cord caused by the volume used in intraparenchymal injections have not been studied [5]. In this review, all experimental studies are based on severely injured spinal cords prior to treatment, and the effect of volume alone cannot be ascertained. Because the spinal cord is confined in a closed space within the dural sac within the osseous vertebral canal, the effects of volume used

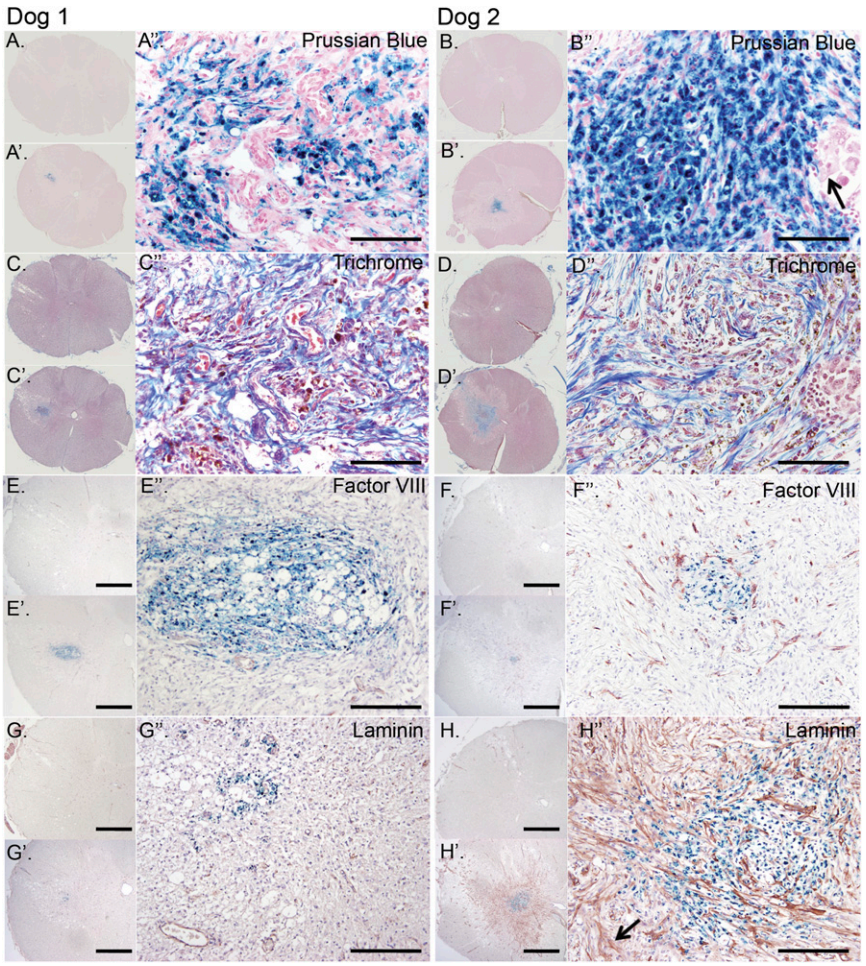

Figure 4. Morphology of canine epidermal neural crest stem cell (cEPI-NCSC) implants in the healthy spinal cord. **(A):** Beagle 1, T12 segment, sham injection. No iron stain is present (Perls' Prussian Blue [PPB]). **(A′):** Beagle 1, L2 segment, cEPI-NCSC injection. Labeled cells are readily identified by blue-stained pigment in the cytoplasm (PPB). **(A′′):** Higher magnification of **(A′)**. Scale bar = 200 μm. **(B):** Beagle 2, T12 segment, sham injection. No iron stain is present (PPB). **(B′):** Beagle 2, L2 segment, cEPI-NCSC injection. Similar to **(A′)**, labeled cells are readily identified by blue-stained pigment in the cytoplasm (PPB). **(B′′):** Higher magnification of **(B′)**. Note that there are few foreign body type multinucleated giant cells (arrow). Scale bar = 200 μm. **(C):** Beagle 1, T12 segment, sham injection. There is an absence of collagen at the injection site (Masson's trichrome [MT]). **(C′):** Beagle 1, L2 segment, cEPI-NCSC injection. Collagen (blue) is present in the implant and is deeply associated with vascular structures (MT). **(C′′):** Higher magnification of **(C′)**. Scale bar = 200 μm. **(D):** Beagle 2, T12 segment, sham injection, MT. There is an absence of collagen at the injection site. **(D′):** Beagle 2, L2 segment, cEPI-NCSC injection. Collagen (blue) is associated with vascular structures (MT). **(D′′):** Higher magnification of **(D′)**. Scale bar = 200 μm. **(E):** Beagle 1, T12 segment, sham injection. Factor VIII expression is associated with few orderly oriented vascular structures (factor VIII immunohistochemistry). Scale bar = 1 mm. **(E′):** Beagle 1, L2 segment, cEPI-NCSC injection. Abundant haphazardly arranged vessels express factor VIII (factor VIII immunohistochemistry). Scale bar = 1 mm. **(E′′):** Higher magnification of **(E′)**. Scale bar = 200 μm. **(F):** Beagle 2, T12 segment (sham injection). Few vessels express factor VIII (factor VIII immunohistochemistry). Scale bar = 1 mm. **(F′):** Beagle 2, L2 segment, cEPI-NCSC injection. Numerous discreet vessels express factor VIII (factor VIII immunohistochemistry). Scale bar = 1 mm. **(F′′):** Higher magnification of **(F′)**. Scale bar = 200 μm. **(G):** Beagle 1, T12 segment, sham injection. Laminin expression is observed in few reactive vessels at the injection site (laminin immunohistochemistry). Scale bar = 1 mm. **(G′):** Beagle 1, L2 segment, cEPI-NCSC injection. Laminin expression present exclusively in numerous reactive vessels (aminin immunohistochemistry). Scale bar = 1 mm. **(G′′):** Higher magnification of **(G′)**. Scale bar = 200 μm. **(H):** Beagle 2, T12 segment, sham injection. Few vessels express laminin (laminin immunohistochemistry). Scale bar = 1 mm. **(H′):** Beagle 2, L2 segment, cEPI-NCSC injection. In addition of reactive vessels, numerous spindle cells (arrow) express laminin at the injection site (laminin immunohistochemistry). Scale bar = 1 mm. **(H′′):** Higher magnification of **(H′)**. Scale bar = 200 μm.

with intraparenchymal injection is valid because the volume of the implanted cells alone may contribute to injury. In this study, we used a lower volume than that reported in any experimental study, even taking into account a total of four injections. If the subtle changes that were seen with objective gait analysis represent the effects of injury caused by the pressure caused by volume within the spinal cord, it must be concluded that using the smallest volume possible is paramount for effective treatment. In an acute SCI model, the spinal cord will be swollen as a function of edema, hemorrhage, and inflammation caused by primary and secondary injury mechanisms. The effect of the volume of a transplant will be even more important in avoiding contributing to the injury. Because the dogs improved clinically on the subjective scales that were used, it is unlikely that the changes in objective gait analysis were a function of the effects of stem cells themselves; that is, this was not a toxicity caused by the stem cells. Clinical neurologic tests also did not detect any measurable

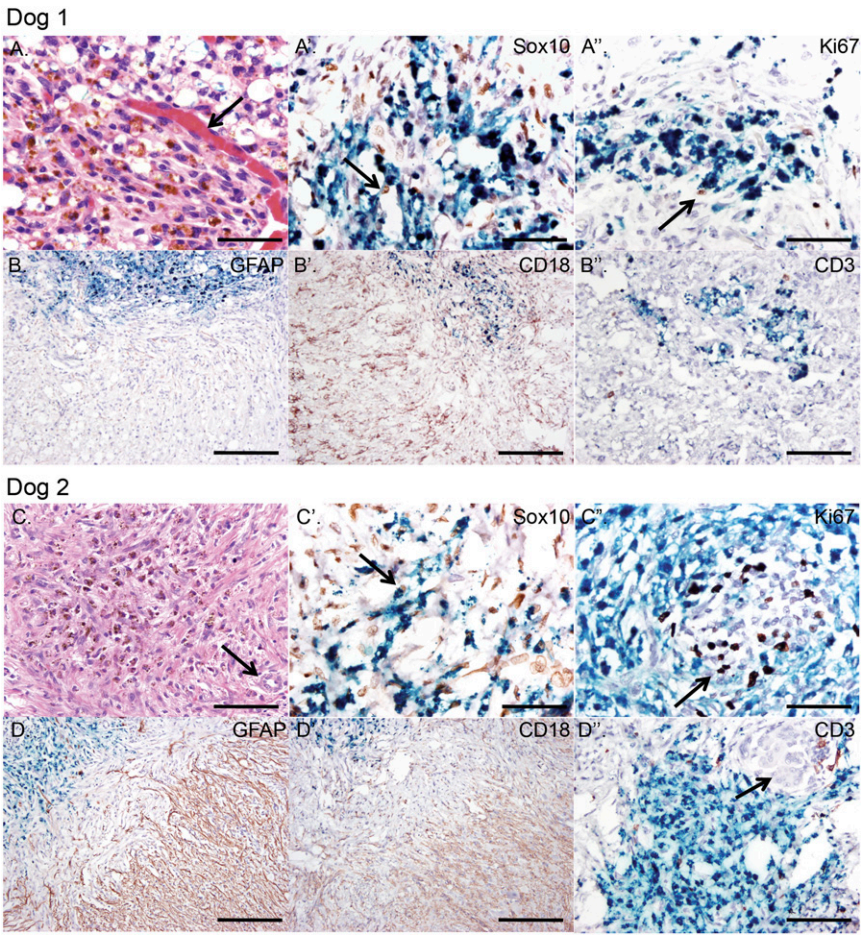

Figure 5. Phenotype of canine epidermal neural crest stem cells (cEPI-NCSCs) and cellular reaction in spinal cord implants. **(A, B):** Dog 1. **(A):** Labeled cEPI-NCSCs are associated with blood vessels (arrow; H&E). Scale bar = 50 μm. **(A′):** Labeled cEPI-NCSCs coexpress iron and the neural crest marker Sox 10 (arrow; double stain, Sox 10 immunohistochemistry, and Perls' Prussian Blue). Scale bar = 50 μm. **(A′′):** cEPI-NCSCs are not proliferating. The proliferation marker Ki67 is only being expressed in reactive lymphocytes (arrow; double stain, Ki67 immunohistochemistry, and Perls' Prussian Blue). Scale bar = 50 μm. **(B):** Mild numbers of reactive astrocytes surround implant (glial fibrillary acidic protein [GFAP] immunohistochemistry). Scale bar = 200 μm. **(B′):** Mild numbers of reactive microglial cells surround the implant (double stain, CD18 immunohistochemistry, and Perls' Prussian Blue). Scale bar = 200 μm. **(B′′):** Few scattered T-lymphocytes are observed at the implant site (double stain, CD3 immunohistochemistry, and Perls' Prussian Blue). Scale bar = 100 μm. **(C, D):** Dog 2. **(C)**: Labeled cEPI-NCSCs are associated with blood vessels (arrow) and numerous plump spindle cells (H&E). Scale bar = 50 μm. **(C′)**: Labeled cEPI-NCSCs coexpress iron and the neural crest marker Sox 10 (arrow; double stain, Sox 10 immunohistochemistry, and Perls' Prussian Blue). Scale bar = 50 μm. **(C′′)**: cEPI-NCSCs are not proliferating. The proliferation marker Ki67 expressed in a cluster of reactive lymphocytes (arrow; double stain, Ki67 immunohistochemistry, and Perls' Prussian Blue). Scale bar = 50 μm. **(D):** Moderate numbers of reactive fibrillary astrocytes surround the implant (double stain, GFAP immunohistochemistry, and Perls' Prussian Blue). Scale bar = 200 μm. **(D′):** Moderate numbers of reactive microglia cells surround implant (double stain, CD18 immunohistochemistry, and Perls' Prussian Blue). Scale bar = 200 μm. **(D′′):** Several T-lymphocytes are observed at the implant site. Note few multinucleated giant cells (arrow; double stain, CD3 immunohistochemistry, and Perls' Prussian Blue). Scale bar = 100 μm.

irreversible adverse effects in spinal cord function during the course of the study. Undoubtedly, the recovery potential in a normal spinal cord is much greater than that of an injured spinal cord.

The spatial resolution of MRI allows for noninvasive monitoring of the graft in the live animal [29, 30]. In rodent models of SCI, magnetic tracing has been performed and was determined to be useful for evaluating cell migration [31]. To date, in vivo tracking of stem cells in the spinal cords of dogs has not been reported [5]. However, stem cell tracking within the dog's central nervous system, in particular in the brain, is generally accepted [32, 33].

Iron oxide nanoparticles are commonly used as magnetic labeling agents of stem cells for in vivo cell tracking [34, 35]. Similar to other studies, we noted that the extent of iron oxide labeling of cEPI-NCSCs was dependent on the iron concentration [36]. Safety tests of nanoparticle products are in general performed by the manufacturers. Safety tests are focused on toxicity studies, confirming the distribution of particle size and standardizing the particle surface coating [37]. Recently, the metabolism and distribution of iron nanoparticles in human mesenchymal stem cells was reported [38]. Superparamagnetic iron particles were stable and packed within endosomes or lysosomes in the cytoplasm, which made these particles ideal probes for in vivo stem cell tracking by MRI. In our study, cEPI-NCSC iron particles were clearly traced for up to 3 weeks in the live animal.

We confirmed by MRI the proper intraparenchymal injection of the cEPI-NCSCs at three of the four injection sites and the

Table 2. Immunohistochemical summary of cEPI-NCSC implants

	Beagle 1		Beagle 2	
Marker	cEPI-NCSCs	Tissue reaction	cEPI-NCSCs	Tissue reaction
Stem cell markers				
Sox10	+/−	+/−	+/−	+/−
Nestin	−	−	−	−
Neural markers				
βIII-Tubulin	−	−	−	−
Synaptophysin	−	−	−	−
GFAP	−	+	−	++
MBP	−	−	−	−
Smooth muscle marker				
SMA	−	+	−	+
Melanocyte marker				
MITF	−	−	−	−
Endothelial marker				
Factor VIII	−	+	−	+
CD31	−	+	−	+
Basal lamina marker				
Laminin	−	+	−	++
Mesenchymal marker				
Vimentin	−	+	−	+
Leukocyte marker				
CD18	−	+	−	++
CD3	−	+	−	+
Proliferation marker				
Ki67	−	+/−	−	+/−

Abbreviations: +, positive immunoreactivity; −, no detectable immunoreactivity; +/−, weak immunoreactivity; cEPI-NCSCs, canine epidermal neural crest stem cell; GFAP, glial fibrillary acidic protein; MBP, myelin basic protein; MITF, microphthalmia transcription factor; SMA, smooth muscle actin.

extradural location of the fourth injection. Because of their sensitivity to the susceptibility artifact, the gradient echo sequences are the preferred MRI sequences for the detection of iron oxide-labeled cells. The MERGE sequence is more sensitive than the SPGR sequence, which explains the difference in size of the area of signal void. The use of an additional T2 FSE sequence was of great value because this sequence permitted even better assessment of the location of the iron-labeled cEPI-NCSCs and of the surrounding spinal cord parenchyma. The T2 hyperintense rim surrounding the injection site at day 2 suggested the presence of edema and/or inflammation secondary to cell injection. A limitation of MRI tracking of iron oxide-labeled cells is the inability to perform quantification. The persistence of the signal void at the sites of injection over time, however, suggests that the label remains at this site. The imaging technique does not distinguish between intracellular iron oxide and interstitial label; however, one would not expect free iron oxide to remain at the site of injection for longer than 2 weeks [38]. For this reason, having only a small reduction in the area of signal void over a 3-week period suggests that most of the cells remain in situ. Notably, similar tissue damage was observed in sham and treatment injections, suggesting that the stem cell graft did not have a deleterious effect on the spinal cord. In an effort to limit the injury created by the transplantation process itself, we used very small injection volumes over an extended period of time. Overall, Wallerian-like axonal degeneration with secondary myelin degeneration is likely to be associated with the iatrogenic grafting procedure, including needle gauge size and volume of injection, rather than being due to the stem cell graft itself.

The general morphology of cEPI-NCSC implants in the canine spinal cord was analogous to our previous data in murine models of SCI [12, 13, 16]. Grafted cEPI-NCSCs integrated into the parenchyma, survived, were not migratory, did not proliferate, and did not form tumors. From our murine models, unilateral transplants lead to bilateral functional improvements, suggesting that mechanisms of cell action involve diffusible molecules [16]. EPI-NCSCs in fact express genes that encode growth factors, including neurotrophins, factors that promote angiogenesis and metalloproteases, which promote scar modulation [7]. cEPI-NCSCs variably expressed Sox10, which confirmed their neural crest origin. In contrast to the rodent studies, implanted cEPI-NCSCs did not express neural crest-specific differentiation markers (βIII-tubulin, synaptophysin, and myelin basic protein). This is most likely due to the shorter duration of the current study. Alternatively, the canine spinal environment may not be conducive to cEPI-NCSC differentiation. Our study provides novel pathophysiological insights into the field of stem cells for canine SCI, which may provide important clues into the mechanisms of the behavior of cEPI-NCSCs in the spinal cord, as well as information about the degree of damage caused by volume injection into the spinal cord. It is important to note that a comparable degree of tissue damage was observed in sham controls and treatment injections. Therefore, loss of myelin is secondary to Wallerian degeneration caused by the injection procedure rather than by the stem cell graft. This notion highlights the importance of keeping injection volumes as low as possible and of infusing the cells slowly.

The fairly robust vascular reaction observed at the treatment sites was attributed to the injected cEPI-NCSCs. Both dogs were considered to have similar vascular and glial reactions. The more prominent scar tissue formation noticed in dog 2 led us to hypothesize that cEPI-NCSCs may have secreted angiogenic factors and proteases that affect tissue remodeling. The expression of Vegf1 and Vegf2 and other vasculogenic factors has been shown by gene expression profiling for mouse EPI-NCSCs (GEO number GSE4680 [7]) and human EPI-NCSCs (GEO number GSE42678 [17]). Similar results were obtained in other studies, which demonstrated increased angiogenesis in laboratory models of SCI with human umbilical cord blood stem cells [39, 40] and in grafts of mouse EPI-NCSCs [16]. Angiogenesis is the process of formation of new vasculature from existing vessels. Sprouting angiogenesis is observed in the brain and involves pericyte and endothelial cell migration through stromal matrices [41]. As a process of wound healing, angiogenesis was shown to be beneficial in neurological diseases by decreasing local ischemia and promoting neurogenesis [42, 43].

Inflammation is a common finding in spinal cord injury, with a peak at 24–72 hours postsurgery and lasting up to 10 days. Given the similarity in magnitude of cell response and cell differential (predominance of neutrophils) in the CSF from both dogs, this alteration was considered a result of the transplantation procedure itself and likely not specifically associated with cells. CSF essentially normalized by week 3 on both dogs. Histologically, the degree of parenchymal inflammation at week 3 was minimal to mild at the sites of cEPI-NCSC transplantation. Because grafted

cEPI-NCSCs were autologous, immunosuppression was not performed and therefore is not an issue here. Local inflammation likely is a consequence of the injection procedure, because it was observed in both sham and cEPI-NCSC injections.

Conclusion

Overall, we conclude that cEPI-NCSCs can be expanded ex vivo into large populations of stem cells useful for in vivo use. cEPI-NCSCs can be marked with magnetizable iron oxide particles without detectable negative effects on cell viability. Transplanted cEPI-NCSCs can be traced by MRI allowing evaluation of their persistence and location in the live animal. No clinically significant adverse effects in the spinal cord are associated with transplantation. When grafted into the spinal cord, cEPI-NCSCs survive in the spinal cord tissue, and they have features that may contribute to improving clinical outcomes in canine SCI. Therefore, the use of cEPI-NCSCs in future safety studies in dogs suffering from spontaneous SCI is warranted.

Acknowledgments

We thank the Center for Equine Health, University of California Davis, and Dick and Carolyn Randall. This work was supported by Fundacao para a Ciencia e a Tecnologia (Portugal), Ministerio da Educacao e Ciencia Grant SFRH/BD/64871/2009 (to B.G.M.) and Medical Research Council (U.K.) Grant 22358 (to M.S.-B.). We thank the Anatomic Pathology Service at the William R. Pritchard Veterinary Medical Teaching Hospital, University of California Davis, in particular Monica Kratochvil and Matt Nichols for their excellent technical support. We also thank John Doval at the University of California Davis MediaLab for assistance with illustrations and Teresa Suter for assistance with the photomicrographs. Finally, we thank Naomi Walker at the Borjesson Laboratory for her dedication and technical support.

Author Contributions

B.G.M.: conception and design, financial support, collection and assembly of data, data analysis and interpretation, manuscript writing; M.S. and S.S.: conception and design, data analysis and interpretation, manuscript writing; M.D.M., J.M., and T.C.G.: collection and assembly of data; G.M.: administrative support, collection and assembly of data; D.L.B. and J.A.N.: conception and design, financial support, data analysis and interpretation, final approval of manuscript; M.S.-B.: conception and design, financial support, data analysis and interpretation, manuscript writing, final approval of manuscript; B.K.S.: conception and design, provision of study material and patients, collection and assembly of data, data analysis and interpretation, final approval of manuscript.

Disclosure of Potential Conflicts of Interest

The authors indicated no potential conflicts of interest.

References

1 Bock P, Spitzbarth I, Haist V et al. Spatiotemporal development of axonopathy in canine intervertebral disc disease as a translational large animal model for nonexperimental spinal cord injury. Brain Pathol 2013;23:82–99.

2 Jeffery ND, Hamilton L, Granger N. Designing clinical trials in canine spinal cord injury as a model to translate successful laboratory interventions into clinical practice. Vet Rec 2011; 168:102–107.

3 Jeffery ND, Smith PM, Lakatos A et al. Clinical canine spinal cord injury provides an opportunity to examine the issues in translating laboratory techniques into practical therapy. Spinal Cord 2006;44:584–593.

4 Spitzbarth I, Baumgärtner W, Beineke A. The role of pro- and anti-inflammatory cytokines in the pathogenesis of spontaneous canine CNS diseases. Vet Immunol Immunopathol 2012;147:6–24.

5 McMahill BG, Borjesson DL, Sieber-Blum M et al. Stem cells in canine spinal cord injury–promise for regenerative therapy in a large animal model of human disease. Stem Cell Rev 2015;11:180–193.

6 Sieber-Blum M, Grim M. The adult hair follicle: Cradle for pluripotent neural crest stem cells. Birth Defects Res C Embryo Today 2004; 72:162–172.

7 Hu YF, Zhang ZJ, Sieber-Blum M. An epidermal neural crest stem cell (EPI-NCSC) molecular signature. Stem Cells 2006;24:2692–2702.

8 Gericota B, Anderson JS, Mitchell G et al. Canine epidermal neural crest stem cells: Characterization and potential as therapy candidate for a large animal model of spinal cord injury. Stem Cells Translational Medicine 2014;3:334–345.

9 Sieber-Blum M, Grim M, Hu YF et al. Pluripotent neural crest stem cells in the adult hair follicle. Dev Dyn 2004;231:258–269.

10 Clewes O, Narytnyk A, Gillinder K et al. Human epidermal neural crest stem cells (hEPI-NCSC): Characterization and directed differentiation into osteocytes and melanocytes. Stem Cell Rev 2011;7:799–814.

11 Mujtaba T, Mayer-Proschel M, Rao MS. A common neural progenitor for the CNS and PNS. Dev Biol 1998;200:1–15.

12 Sieber-Blum M, Schnell L, Grim M et al. Characterization of epidermal neural crest stem cell (EPI-NCSC) grafts in the lesioned spinal cord. Mol Cell Neurosci 2006;32:67–81.

13 Sieber-Blum M. Epidermal neural crest stem cells and their use in mouse models of spinal cord injury. Brain Res Bull 2010;83: 189–193.

14 Enzmann GU, Benton RL, Talbott JF et al. Functional considerations of stem cell transplantation therapy for spinal cord repair. J Neurotrauma 2006;23:479–495.

15 Donnelly EM, Lamanna J, Boulis NM. Stem cell therapy for the spinal cord. Stem Cell Res Ther 2012;3:24.

16 Hu YF, Gourab K, Wells C et al. Epidermal neural crest stem cell (EPI-NCSC)-mediated recovery of sensory function in a mouse model of spinal cord injury. Stem Cell Rev 2010;6: 186–198.

17 Narytnyk A, Verdon B, Loughney A et al. Differentiation of human epidermal neural crest stem cells (hEPI-NCSC) into virtually homogenous populations of dopaminergic neurons. Stem Cell Rev 2014;10:316–326.

18 Wesselschmidt RL. The teratoma assay: An in vivo assessment of pluripotency. Methods Mol Biol 2011;767:231–241.

19 Olby NJ, De Risio L, Muñana KR et al. Development of a functional scoring system in dogs with acute spinal cord injuries. Am J Vet Res 2001;62:1624–1628.

20 Budsberg SC, Jevens DJ, Brown J et al. Evaluation of limb symmetry indices, using ground reaction forces in healthy dogs. Am J Vet Res 1993;54:1569–1574.

21 Amit M, Margulets V, Segev H et al. Human feeder layers for human embryonic stem cells. Biol Reprod 2003;68:2150–2156.

22 Levine JM, Levine GJ, Porter BF et al. Naturally occurring disk herniation in dogs: An opportunity for pre-clinical spinal cord injury research. J Neurotrauma 2011;28:675–688.

23 Gropp M, Shilo V, Vainer G et al. Standardization of the teratoma assay for analysis of pluripotency of human ES cells and biosafety of their differentiated progeny. PLoS One 2012; 7:e45532.

24 Paul C, Samdani AF, Betz RR et al. Grafting of human bone marrow stromal cells into spinal cord injury: A comparison of delivery methods. Spine 2009;34:328–334.

25 Garcia T, Sturges BK, Stover SM et al. Forelimb brachial muscle activation patterns using surface electromyography and their relationship to kinematics in normal dogs walking and trotting. Comparative Exercise Physiol 2014;10:13–22.

26 DeCamp CE, Soutas-Little RW, Hauptman J et al. Kinematic gait analysis of the trot in healthy greyhounds. Am J Vet Res 1993;54:627–634.

27 Nordquist B, Fischer J, Kim SY et al. Effects of trial repetition, limb side, intraday and inter-week variation on vertical and craniocaudal ground reaction forces in clinically normal Labrador retrievers. Vet Comp Orthop Traumatol 2011;24:435–444.

28 Ragetly CA, Griffon DJ, Mostafa AA et al. Inverse dynamics analysis of the pelvic limbs in Labrador retrievers with and without cranial cruciate ligament disease. Vet Surg 2010;39:513–522.

29 Bulte JW, Arbab AS, Douglas T et al. Preparation of magnetically labeled cells for cell tracking by magnetic resonance imaging. Methods Enzymol 2004;386:275–299.

30 Bulte JW, Duncan ID, Frank JA. In vivo magnetic resonance tracking of magnetically labeled cells after transplantation. J Cereb Blood Flow Metab 2002;22:899–907.

31 Sykova E, Jendelova P. In vivo tracking of stem cells in brain and spinal cord injury. Prog Brain Res 2007;161:367–383.

32 Walton RM, Magnitsky SG, Seiler GS et al. Transplantation and magnetic resonance imaging of canine neural progenitor cell grafts in the postnatal dog brain. J Neuropathol Exp Neurol 2008;67:954–962.

33 Lu SS, Liu S, Zu QQ et al. In vivo MR imaging of intraarterially delivered magnetically labeled mesenchymal stem cells in a canine stroke model. PLoS One 2013;8:e54963.

34 Laurent S, Forge D, Port M et al. Magnetic iron oxide nanoparticles: Synthesis, stabilization, vectorization, physicochemical characterizations, and biological applications. Chem Rev 2008;108:2064–2110.

35 Mahmoudi M, Hosseinkhani H, Hosseinkhani M et al. Magnetic resonance imaging tracking of stem cells in vivo using iron oxide nanoparticles as a tool for the advancement of clinical regenerative medicine. Chem Rev 2011;111:253–280.

36 Boutry S, Brunin S, Mahieu I et al. Magnetic labeling of non-phagocytic adherent cells with iron oxide nanoparticles: A comprehensive study. Contrast Media Mol Imaging 2008; 3:223–232.

37 Mahmoudi M, Hofmann H, Rothen-Rutishauser B et al. Assessing the in vitro and in vivo toxicity of superparamagnetic iron oxide nanoparticles. Chem Rev 2012;112:2323–2338.

38 Tian F et al. Fates of FeO and FeO@SiO nanoparticles in human mesenchymal stem cells assessed by synchrotron radiation-based techniques. Biomaterials 2014;35:6412–6421.

39 Ning G, Tang L, Wu Q et al. Human umbilical cord blood stem cells for spinal cord injury: Early transplantation results in better local angiogenesis. Regen Med 2013;8:271–281.

40 Park DH, Lee JH, Borlongan CV et al. Transplantation of umbilical cord blood stem cells for treating spinal cord injury. Stem Cell Rev 2011;7:181–194.

41 Plate KH. Mechanisms of angiogenesis in the brain. J Neuropathol Exp Neurol 1999;58:313–320.

42 Krupinski J, Kaluza J, Kumar P et al. Role of angiogenesis in patients with cerebral ischemic stroke. Stroke 1994;25:1794–1798.

43 Rizvanov AA, Kiyasov AP, Gaziziov IM et al. Human umbilical cord blood cells transfected with VEGF and L(1)CAM do not differentiate into neurons but transform into vascular endothelial cells and secrete neuro-trophic factors to support neuro-genesis-a novel approach in stem cell therapy. Neurochem Int 2008;53: 389–394.

44 Executive board actions range from strategic plan to stem cells. Am J Vet Res 2011;72: 1002–1004.

See www.StemCellsTM.com for supporting information available online.